Drug Design, Development and Therapy

Dovepress
Taylor & Francis Group

Open Access Full Text Article

ORIGINAL RESEARCH

Integrated Microbiome and Metabolome Analysis Reveals Correlations Between Gut Microbiota Components and Metabolic Profiles in Mice With Mitoxantrone-Induced Cardiotoxicity

Qing Zhang[1], Deshuai Liang[2], Chengfang Zhang[3], Ling Ye[4], Ping Sun[4], Hongli Zhu[4], Yongqin Zhao[4], Yuewen Li[4], Yun Guan[4], Haiguo Zhang[4]

[1]College of Clinical Medicine, Jining Medical University, Jining, 272013, People's Republic of China; [2]Department of Pharmacy, Jining NO. 1 People's Hospital, Jining, 272000, People's Republic of China; [3]Department of Clinical Laboratory, Jining NO. 1 People's Hospital, Jining, 272000, People's Republic of China; [4]Department of Hematology, Jining NO. 1 People's Hospital, Jining, 272000, People's Republic of China

Correspondence: Haiguo Zhang; Yun Guan, Jining NO. 1 People's Hospital, 6 Jiankang Road, Jining Shandong, 272000, People's Republic of China, Tel/Fax +86-0537 2257626; +86-0537 2087093, Email wfmchero@126.com; gyuanun1989@163.com

Purpose: Mitoxantrone (MTX) is largely restricted in clinical usage due to its significant cardiotoxicity. Multiple studies have shown that an imbalance in the gut-heart axis plays an important role in the development of cardiovascular disease (CVD). We aim to explore the possible correlations between gut microbiota (GM) compositions and cardiometabolic (CM) disorder in MTX-triggered cardiotoxicity mice.

Methods: MTX cumulative dose of 6 mg/kg was administered to healthy Kunming male mice to trigger cardiotoxicity, with 1 mg/kg twice weekly for a duration of 3 weeks. Plasma CK-MB and LDH levels were determined, and the heart tissue histopathology was assessed, followed by utilizing an integrated liquid chromatography-mass spectrometry (LC-MS)-based heart metabolomics study alongside the 16S ribosomal RNA (rRNA) sequencing method to assess MTX impact on GM and CM profiles in mice, establishing associations between GM and CM profiles through the Pearson correlation coefficient calculation.

Results: MTX caused CK-MB and LDH level elevations and cardiotoxicity in our mouse model. MTX primarily affected the processes of protein digestion and absorption, mineral absorption, membrane transport, production of aminoacyl-transfer RNA (tRNA), metabolism of nucleotides, lipids, and amino acids, as well as autophagy. Additionally, MTX increased *Romboutsia, Enterococcus*, and *Turicibacter* abundances and lowered *norank_f__Muribaculaceae, Alistipes, Odoribacter, norank_f__Lachnospiraceae, norank_f__Ruminococcaceae, norank_f__Oscillospiraceae, unclassified_f__Ruminococcaceae, NK4A214_group, Colidextribacter, norank_f__norank_o__Clostridia_vadinBB60_group, Rikenella*, and *Anaerotruncus* abundances. The correlation analyses showcased variations in the abundance of diverse flora, such as *Romboutsia, Enterococcus, Turicibacter, and norank_f__Muribaculaceae*, which were related to MTX-induced cardiac injury.

Conclusion: Our study supports the claim that MTX provokes cardiotoxicity by modifying CM and GM profiles. Our results offer new possibilities for controlling MTX-triggered cardiotoxicity.

Keywords: 16S ribosomal RNA, liquid chromatography-mass spectrometry, mitoxantrone, cardiotoxicity

Introduction

Mitoxantrone (MTX), a chemical belonging to the anthraquinone class, exhibits anti-tumor properties by impeding RNA and DNA synthesis via the process of DNA insertion and topoisomerase II's inhibition.[1–3] It also has powerful immunosuppressive and immunomodulatory properties.[4] MTX has been widely employed in treating leukemia, advanced metastatic breast malignancy, non-Hodgkin's lymphoma, hormone-refractory prostate cancer, and multiple sclerosis.[5] Regrettably, mitoxantrone can cause a variety of adverse reactions such as cardiotoxicity, myelosuppression,

Received: 27 July 2024
Accepted: 15 January 2025
Published: 22 January 2025

hepatotoxicity, and gastrointestinal reactions such as nausea and vomiting, and cardiotoxicity represents a significant and prevalent negative outcome for those treated with MTX.[6] MTX-induced cardiotoxicity is dose-dependent and is characterized by reduced left ventricular ejection fraction along with congestive heart failure and/or dilated cardiomyopathy.[7]

The human microbiome represents an intricate ecosystem that usually contains hundreds to thousands of bacterial species alongside viruses, fungi, and phages. It is continually influenced by the host and its surroundings while being critical in the host's function, health, and diseases.[8] Recent findings have unveiled that the gut microbiome (GM) comprises a total of 2172 distinct species distributed across 12 different phyla. The majority of these species fall under *Verrucomicrobia, Proteobacteria, Bacteroidetes, Firmicutes*, and *Actinobacteria* phyla. Mainly, *Firmicutes* and *Bacteroidetes* constitute the two predominant microbes, collectively constituting about 90% of the population.[9] Recent metagenomics and metabolomics studies have revealed that GM and its related metabolites may serve as probable cardiovascular disease (CVD) risk factors.[10] The change in *Firmicutes-Bacteroidetes* (F/B) ratio and gut microbial metabolite imbalance, which comprises trimethylamine N-oxide (TMAO) and short-chain fatty acids (SCFAs), are essential in CVD pathogenesis.[11] SCFAs, comprising butyrate, acetate, and propionate, have essential functions in preserving intestinal barrier integrity, blood pressure regulation, glucose and lipid metabolism, anti-inflammatory responses, and immune system modulation.[12] SCFAs can exhibit their anti-inflammatory potential by inhibiting histone deacetylase (HDAC) activity and specific G-protein coupled receptor (GPCR) activation.[13]

Currently, there is no effective treatment or preventive measure for MTX-triggered cardiac damage. Accordingly, seeking a treatment to alleviate MTX-induced heart failure or cardiomyopathy is crucial. MTX causes cardiotoxicity through a variety of pathways, but the exact regulatory mechanisms remain undefined until now.[14–18] The GM has been elucidated to impact CVD occurrence and development, and the change in GM composition can provide new and promising opportunities for the treatment of CVD.[19] Nutritional interventions have been found to significantly affect the composition of the gut microbiota. A diet high in fiber and short-chain fatty acids is linked to lower gut dysbacteriosis in patients with heart failure, while a diet low in fiber is linked to negative cardiac remodeling, which leads to hypertension and the progression of cardiac fibrosis.[20,21] Probiotics may be an additional treatment option for avoiding CVD. It is known that probiotics are bacteria whose consumption and subsequent interaction with gut flora may result in numerous benefits in terms of cardiac protection and anti-inflammatory reactions.[22] Herein, an integrated liquid chromatography-mass spectrometry (LC-MS)-dependent metabolomics alongside 16S ribosomal RNA (rRNA) sequencing was employed, aiming at elucidating probable correlations between GM components and cardiometabolic (CM) biomarkers following MTX exposure. Accordingly, we elucidate the understanding of MTX-provoked cardiotoxicity and establish a foundation for innovative approaches to its therapy.

Materials and Methods

Chemicals and Reagents

MTX hydrochloride (purity > 98%) and 2-chloro-L-phenylalanine (purity ≥ 98%) were procured from Macklin Biochemical (Shanghai, China). Methanol and acetonitrile (both HPLC grade) and water (LC-MS grade) were obtained from Fisher Chemical (Shanghai, China), while formic acid (HPLC grade) was from CNW (Shanghai, China). Our study procured 2-propanol (HPLC grade) from Merck (Darmstadt, Germany). All experimental procedures followed the Use of Laboratory Animal Guidelines and were authorized by the Animals Experimentation of the Jining NO.1 People's Hospital Ethical Committee (2023DW090).

Animals and Treatment

Following one week of acclimating Kunming male mice (n = 14; 5 weeks old; 30–35g; Pengyue Experimental Animal Breeding, Jinan, China; approval number: SCXK20190003) at 20 ± 2 °C and 65% humidity at a 12-h light-dark cycle with free food and water access, they were assigned at random into the control (n = 6) and MTX groups (n = 8). The MTX administration protocol was designed to closely resemble human cancer therapy, as it involved administering the medicine in cycles and through many administrations.[16] The mice were intraperitoneally injected with 6 mg/kg of MTX

twice weekly for a duration of 3 weeks. Each administration consisted of 1 mg/kg, with alternating injections between the left and right abdomen side to minimize additional harm and pain.[16] The MTX hydrochloride went through dissolving in a sterile solution of 0.9% saline. The overall cumulative dose administered was equal to a human dosage of 36.3 mg/m^2.[16] Control mice received an injection of a saline solution containing 0.9% NaCl in an equivalent volume and under the same circumstances as the mice who received MTX treatment. The injections were given in the afternoon because mice have lower susceptibility to MTX toxicity during that time period.[16]

Sample Collection and Preparation

Following completing the MTX challenge interval, the mice were administered anesthesia using 1% sodium pentobarbital (50 mg/kg). After removing the eyeballs, blood samples were collected from each mouse. After being centrifuged at 4000 rpm for 10 min at 4 °C, we maintained serum samples at −80 °C until analysis. Cervical dislocation was used to sacrifice the animals. Following that, the liver and heart were removed, and the partial heart samples went through rapid freezing with liquid nitrogen and kept at −80 °C. Within sterile conical tubes, the colon contents were gathered.

A 50 mg sample of heart tissue was placed into a centrifuge tube with a volume of 2 mL. Additionally, a grinding bead with a diameter of 6 mm was added. For metabolite extraction, we then employed 400 μL of extraction solution (methanol: water = 4: 1 (v: v)) that contained 0.02 mg/mL of internal standard (L-2-chlorophenylalanine). Using the Wonbio-96c frozen tissue grinder (Shanghai Wanbo Biotechnology Co., LTD), the samples were pulverized for 6 min (−10°C, 50 hz), extracted using low-temperature ultrasonication for 30 min (5°C, 40 kHz), and incubated for 30 min at −20°C. After that, they were subjected to centrifugation for 15 min (4°C, 13000 g), transferring the resulting supernatant into the injection vial to conduct LC-MS analysis. Ultimately, we combined 20 μL of each sample within either group to be the quality controls (QC).

Determining Cardiotoxicity and Hepatoxicity Indicator

Our study assessed serum creatine kinase (CK)-MB, lactate dehydrogenase (LDH), aspartate (AST) and alanine aminotransferase (ALT), employing the specific kits (Jiancheng Bioengineering Institute, Nanjing, China) through a spectrophotometer per the instructions (UNICO Instruments, Model 1200, USA).

Histopathological Investigation

The remaining heart and liver samples underwent dehydration using ethanol and xylene, followed by paraffin embedding, sectioning at 5 μM, and Hematoxylin and Eosin (H&E) staining for histological inspection. We utilized a 3D panoramic scanner (HISTECH Panoramic 250, Hungary) to examine the stained heart and liver sections and determine the areas displaying pathological alterations.

Flow Cytometry

The remaining liver tissues were ground to make cell suspensions, and the liver lymphocyte subsets were detected using a flow cytometer (Beckman DXFLEX) after antibody dressing, centrifugation, washing with PBS buffer, and lysis with erythrocyte lysate.

LC-MS-Based Metabolomics Analysis

The sample analysis was carried out by LC-MS on a Thermo UHPLC-Q Exactive HF-X system containing an ACQUITY HSS T3 column (Majorbio Bio-Pharm Technology Co. Ltd., Shanghai, China). Solvent A: 0.1% formic acid in (water: acetonitrile = 95: 5, (v/v)) alongside solvent B: 0.1% formic acid in (acetonitrile: isopropanol: water = 47.5: 47.5: 5, (v/v/v)) constituted the mobile phases. The volumes used for sample injection were 3 μL, with a 0.40 mL/min flow rate and 40 °C column temperature. We acquired the mass spectrometric data by employing the Thermo UHPLC-Q Exactive HF-X MS containing an electrospray ionization source operating in positive and negative modes. The detection was conducted using a 70–1050 mass-to-charge (m/z) full scan range.

Data Processing and Multivariate Analysis

The LC/MS raw data was preprocessed through Progenesis QI software (Waters Corporation, Milford, USA), exporting the resulting data as a three-dimensional (3D) data matrix in CSV format that contained sample information, mass spectral response intensity, and metabolite names. Our study identified the metabolites by scanning the HMDB (http://www.hmdb.ca/), Metlin (https://metlin.scripps.edu/), and Majorbio Databases.

Our study uploaded the acquired data matrix to the Majorbio cloud (https://cloud.majorbio.com), enabling data analysis. Initially, the data matrix underwent pre-processing in the following manner: A minimum of 80% of the metabolic characteristics identified in each given group of samples were preserved. Following the application of a filter, the lowest value of metabolite levels was computed for individual samples that fell under the lower quantification limit, normalizing each metabolic signature to the sum. For error mitigation resulting from sample preparation and instrument instability, we standardized the MS peak response intensities in the sample through the sum normalization approach, forming a normalized data matrix. QC samples having a relative standard deviation (RSD) > 30% were eliminated and then transformed using a log10 logarithmic function to create the final data matrix utilized to conduct further analysis.

Subsequently, principal component analysis (PCA), as well as orthogonal least partial squares discriminant analysis (OPLS-DA), was carried out by developing the R package "ropls" (Version 1.6.2), comparing both groups utilizing two-tailed Student's *t*-tests. Our study identified metabolites that matched the criteria of having variable importance in projection (VIP) > 1.0 and two-tailed Student's *t*-test $p < 0.05$ as probable differentially expressed metabolites (DEMs). Mapping the differential metabolites to their respective biochemical pathways was conducted via the KEGG database's metabolic enrichment and pathway analysis (http://www.genome.jp/kegg/), deploying the "scipy.stats" Python package (https://docs.scipy.org/doc/scipy/) for enrichment analysis, aiming at identifying the most pertinent biological pathways regarding MTX treatment.

16S rRNA Sequencing of GM

We carried out 16S rRNA sequencing analysis employing Majorbio Bio-Pharm Technology (Shanghai, China). Our study obtained the microbe genomic DNA from the colon contents through the FastPure Feces DNA Isolation Kit (Majorbio Bio-Pharm Technology Co. Ltd., Shanghai, China). Utilizing 1% agarose gel electrophoresis, we then separated the DNA fragments. The V3–V4 hyper-variable portions of the bacterial 16S rRNA gene amplification was performed employing TransStart Fastpfu DNA Polymerase (TransGen AP221-02) through a PCR system (Gene Amp 9700, ABI, USA). Afterward, the PCR product sequences were extracted, purified, and sequenced via NextSeq™1000/2000 P1 Reagents (600 cycles) employing an Illumina Nextseq 2000 platform (both from Illumina, USA). Moreover, we acquired the raw data following the RS_ReadsOfinsert1 protocol, utilizing the QIIME software (Version 1.9.1, http://qiime.org/install/index.html) for acquiring sequences of high-quality. Employing UPARSE (version 7.1), the analysis of operational taxonomic units (OTUs) clustering possessing a 97% similarity threshold was performed. Additionally, we discovered and eliminated any chimeric sequences. Herein, we utilized the Ribosomal Database Program classifier Bayesian algorithm for taxonomic analyses of species against the Silva 16S rRNA database, employing a 70% confidence threshold. Subsequently, we conducted alpha and beta diversity studies and community composition analysis. We employed the Phylogenetic Investigation of Communities by Reconstruction of Unobserved States (PICRUSt) 2 (version 1.1.0, http://picrust.github.io/picrust/) tool to anticipate orthologous group (COG) cluster functions. In order to evaluate potential correlations between GM components and CMs, a Pearson correlation heatmap was created.

Results

MTX-Triggered Cardiotoxicity and Hepatoxicity in a Mouse Model

Plasma CK-MB level was significantly higher in the MTX-treated mice than in the control mice (Figure 1A, $p < 0.001$). Additionally, a tendency for increased LDH of the MTX-treated group, compared with the control, was observed (Supplementary Figure 1). The qualitative histologic examination of the heart of MTX-treated mice and controls was done using the H&E staining. The control group histologic sections showed normal morphology and structure

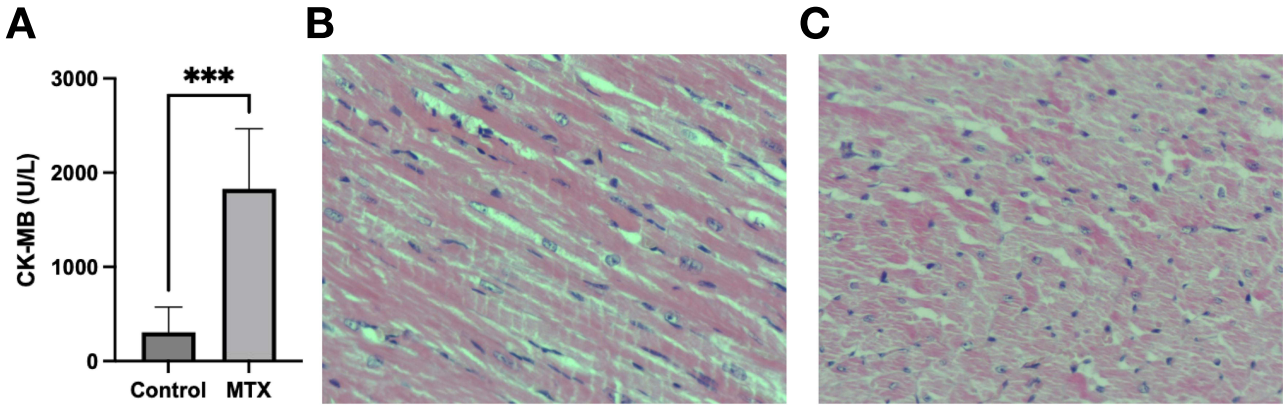

Figure 1 MTX-induced cardiotoxicity in a mouse model. (**A**) CK-MB serum levels of challenged and control mice. HE staining images showing histopathological features of (**B**) control and (**C**) MTX mice. ***$p < 0.001$ represents statistically significant differences between the control and MTX groups.

(Figure 1B). However, cardiomyocytes from the challenge group are swollen and disordered with enlarged nuclei and pale cytoplasm (Figure 1C). These results indicate that MTX caused cardiotoxicity in our model mice. AST and ALT levels were more elevated in the peripheral blood serum of the MTX mouse than the control but with a nonsignificant difference (Supplementary Figure 2A and B), which was assessed to explore whether the MTX triggered hepatoxicity in a mouse model. Furthermore, we studied the liver injury of the MTX and control mice by using H&E staining. The histologic sections of the control group exhibited normal hepatocyte morphology without any detectable changes (Supplementary Figure 2C). Nonetheless, the ballooning and hydropic degeneration happened in liver cells, the cell nucleus was broken and disintegrated, and spotty and flaky necrosis even occurred in the MTX mouse (Supplementary Figure 2D). The MTX mouse showed a tendency towards elevated serum ALT and AST levels, suggesting liver damage. Nevertheless, these differences were not statistically significant in comparison to the control mouse, probably because of the limited sample size.

CM Profiles of MTX-Provoked Mice by LC-MS

Aiming at determining the MTX influence on CM profiles, an LC-MS-dependent untargeted metabolomics was applied. Our Venn diagram analysis results showed relatively small variations between both groups in metabolite species (Figure 2A and B). Nonetheless, the OPLS-DA model results demonstrated clear discrepancies between the two groups (Figure 2C and D). The parameters derived from 200 test permutations demonstrated the reliability of the OPLS-DA models and predictions (Figure 2E and F, and Table 1).

We identified metabolites with a VIP score of more than 1 from the OPLS-DA along with $p < 0.05$ from Student's *t*-tests as prospective biomarkers that may be accountable for the observed variations between both groups. The volcano plot result showed 97 DEMs: 30 were overexpressed, and 67 were suppressed (Figure 3A). Supplementary Table 1 summarizes the top 30 DEMs by VIP values while listing the remaining 67 DEMs in Supplementary Table 2. Figure 3B displays the cluster analysis of the top 30 DEMs of the control and MTX groups, showing overexpression of various long-chain and very-long-chain (VLC)-acylcarnitines (ACs), partial medium-chain ACs, Delta-Tetradecalactone, 4-Methylumbelliferone, 2-Thiothiazolidine-4-carboxylic acid, (3s)-3-(Benzyloxy)-L-Aspartic Acid, and METENEPROST, while those of various gut microbial metabolites, various SC-ACs, partial medium-chain ACs, 4-Methylumbelliferone glucuronide, 2.4-Hexadienyl acetate, Dihomo-alpha-linolenic acid, Gamma-Glutamylvaline, 3-hydroxy-3-(3-hydroxyphenyl)propanoic acid (PA)-O-sulphate, Bufadienolide, LysoPA(20:4(8Z,11Z,14Z,17Z)/-0:0), Tiopronin, Curdione, Naepaine, Aspartame, oxidized polyethylene (Polyethylene, oxidized), and (3R,4R,5R)-3-Fluoro-5-(hydroxymethyl)oxolane-2,3,4-triol were downregulated after MTX treatment. Figure 3D-G depicts the box plots of three downregulated gut microbial metabolites and one upregulated long-chain AC distribution in each group of samples after the MTX challenge. In addition, the DEMs underwent pathway analysis, which revealed that MTX treatment had an impact on various biological processes, including nutrient digestion and absorption, central carbon and choline

https://doi.org/10.2147/DDDT.S479682

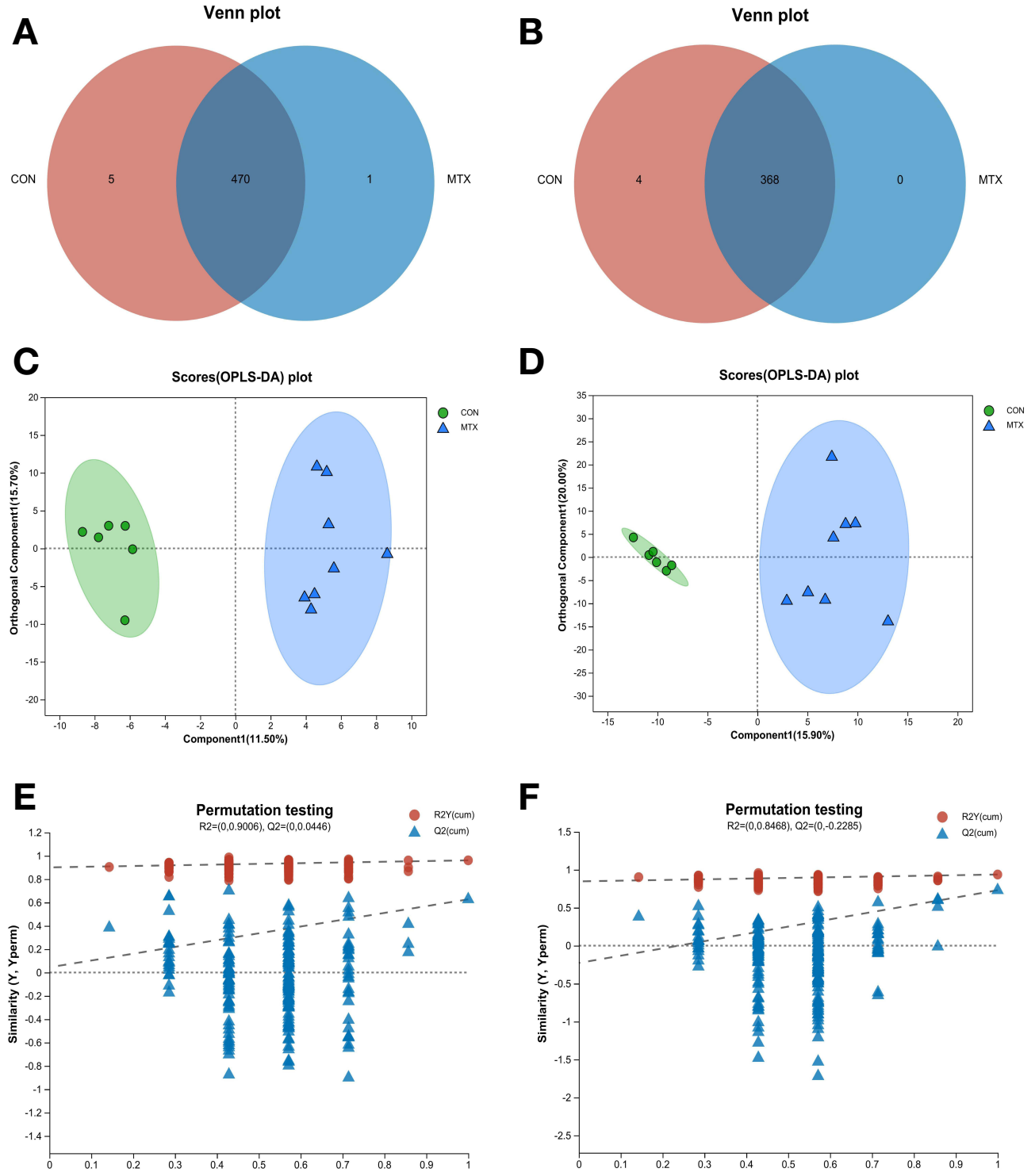

Figure 2 Metabolomic analysis of heart tissues between the control and MTX groups. The Venn diagram analysis of quantified metabolites in positive ion mode (**A**) and negative ion mode (**B**). OPLS-DA scores plots in positive ion mode (**C**) and negative ion mode (**D**). 200 permutation tests of OPLS-DA models in positive ion mode (**E**) and negative ion mode (**F**).

metabolism within malignancies, ATP-binding cassette transporters, aminoacyl-transfer RNA (tRNA) biosynthesis, glycerophospholipid, nucleotide, pyrimidine, and amino acids metabolism, kaposi sarcoma-related herpesvirus infection, autophagy, and glycosylphosphatidylinositol (GPI)-anchor biosynthesis (Figure 3C and Supplementary Table 3).

https://doi.org/10.2147/DDDT.S479682

Table 1 OPLS-DA Model Validation Parameters Between Groups

Group	Mode	R2X (cum)	R2Y (cum)	Q2 (cum)
CON vs MTX	positive ion	0.272	0.961	0.627
CON vs MTX	negative ion	0.36	0.937	0.73

MTX-Triggered GM Changes

The 16S RNA sequencing analysis results revealed declines in community richness and diversity post-MTX challenge (alpha-diversity indices Chao, Ace, Shannon, and Simpson) (Figure 4A-D). The Good's coverage index, which measures the detected sample coverage, demonstrated that the sequencing depth accurately represented GM (Figure 4E). The principal coordinates analysis at the OTU level (Bray-Curtis distance algorithm and ANOSIM analysis), which assessed beta diversity, revealed a significant distinction between both groups. Furthermore, the intergroup disparities were significantly larger than the intragroup variations (Figure 4F).

The Venn diagram displayed a total of 910 OTUs across all groups, with a similarity threshold of 97%. The control and MTX groups included 273 and 147 distinct OTUs, respectively (Figure 4G). The community barplot analysis results (Figure 4H) showcased the major GM components in the control group to be *Firmicutes* (59.98%), *Bacteroidota* (25.43%), *Patescibacteria* (5.43%), *Actinobacteriota* (5.07%), *Desulfobacterota* (3.50%), *verrucomicrobiota* (0.10%), and *Proteobacteria* (0.06%) at the phylum level; with *verrucomicrobiota* (12.26%), *Proteobacteria* (9.63%), and *Actinobacteriota* (5.16%) abundances being elevated and those of *Firmicutes* (59.54%), *Bacteroidota* (9.70%), *Patescibacteria* (2.69%), and *Desulfobacterota* (0.90%) being reduced in the MTX group. GM pre-MTX challenge mainly comprised *Lactobacillus* (25.20%), *norank_f__Muribaculaceae* (10.57%), *Alistipes* (5.60%), *Candidatus_Saccharimonas* (5.43%), *Lachnospiraceae_NK4A136_group* (4.39%), *norank_f__norank_o__Clostridia_UCG-014* (4.32%), *Enterorhabdus* (4.26%), and *Akkermansia* (0.10%) at the genus level; and after the challenge, *Lactobacillus* (26.03%), *Akkermansia* (12.26%), *Romboutsia* (9.23%), *Escherichia-Shigella* (9.13%), *norank_f__norank_o__Clostridia_UCG-014* (5.82%), and *Enterorhabdus* (4.27%) abundances increased, while *norank_f__Muribaculaceae* (4.75%), *Candidatus_Saccharimonas* (2.69%), *Lachnospiraceae_NK4A136_group* (2.62%), and *Alistipes* (0.41%) abundances decreased (Figure 4I). The 16S rRNA sequencing data analysis, alongside the COG databases, allowed us to anticipate the primary functions of the bacteria. These functions were found to be primarily related to metabolism, with amino acid metabolism being the most abundant (Figure 4J).

The Comparisons of GM Species Population

Figure 5A depicts that the calculated F/B ratio exhibited a significant rise in the MTX (6.14) group compared to the control (2.36) group. We conducted a statistical analysis aiming at comparing the populations of various species between both groups. This analysis was executed employing the Wilcoxon rank-sum test to identify any significant changes. The MTX group mice exhibited reduced *Bacteroidota* amounts at the phylum level ($p < 0.05$; Figure 5B). At the genus level, *norank_f__Muribaculaceae* ($p < 0.05$), *Alistipes* ($p < 0.01$), *Odoribacter* ($p < 0.01$), *norank_f__Lachnospiraceae* ($p < 0.05$), *norank_f__Ruminococcaceae* ($p < 0.01$), *norank_f__Oscillospiraceae* ($p < 0.01$), *unclassified_f__Ruminococcaceae* ($p < 0.01$), *NK4A214_group* ($p < 0.05$), *Colidextribacter* ($p < 0.01$), *norank_f__norank_o__Clostridia_vadinBB60_group* ($p < 0.01$), *Rikenella* ($p < 0.05$), and *Anaerotruncus* ($p < 0.05$) abundances possessed a significant decrease in the MTX group. Meanwhile, *Romboutsia* ($p < 0.01$), *Enterococcus* ($p < 0.05$), and *Turicibacter* ($p < 0.05$) amounts showed a remarkable increase in the MTX group mice (Figure 5C). In order to identify the candidate species responsible for MTX-provoked cardiotoxicity, we conducted linear discriminant analysis (LDA) effect size and successfully identified 34 differential species (Supplementary Figure 3). Notably, LDA scores revealed that *Romboutsia* and *norank_f__Muribaculaceae* were the top two genera (Supplementary Table 4).

Relevance Analysis Between CM Biomarkers and GM

The results of calculating the Pearson correlation coefficient showcased that *Bacteroidota* and some bacteria at the genus levels, including *norank_f__Muribaculaceae, Romboutsia, Alistipes, Odoribacter, norank_f__Lachnospiraceae,*

https://doi.org/10.2147/DDDT.S479682

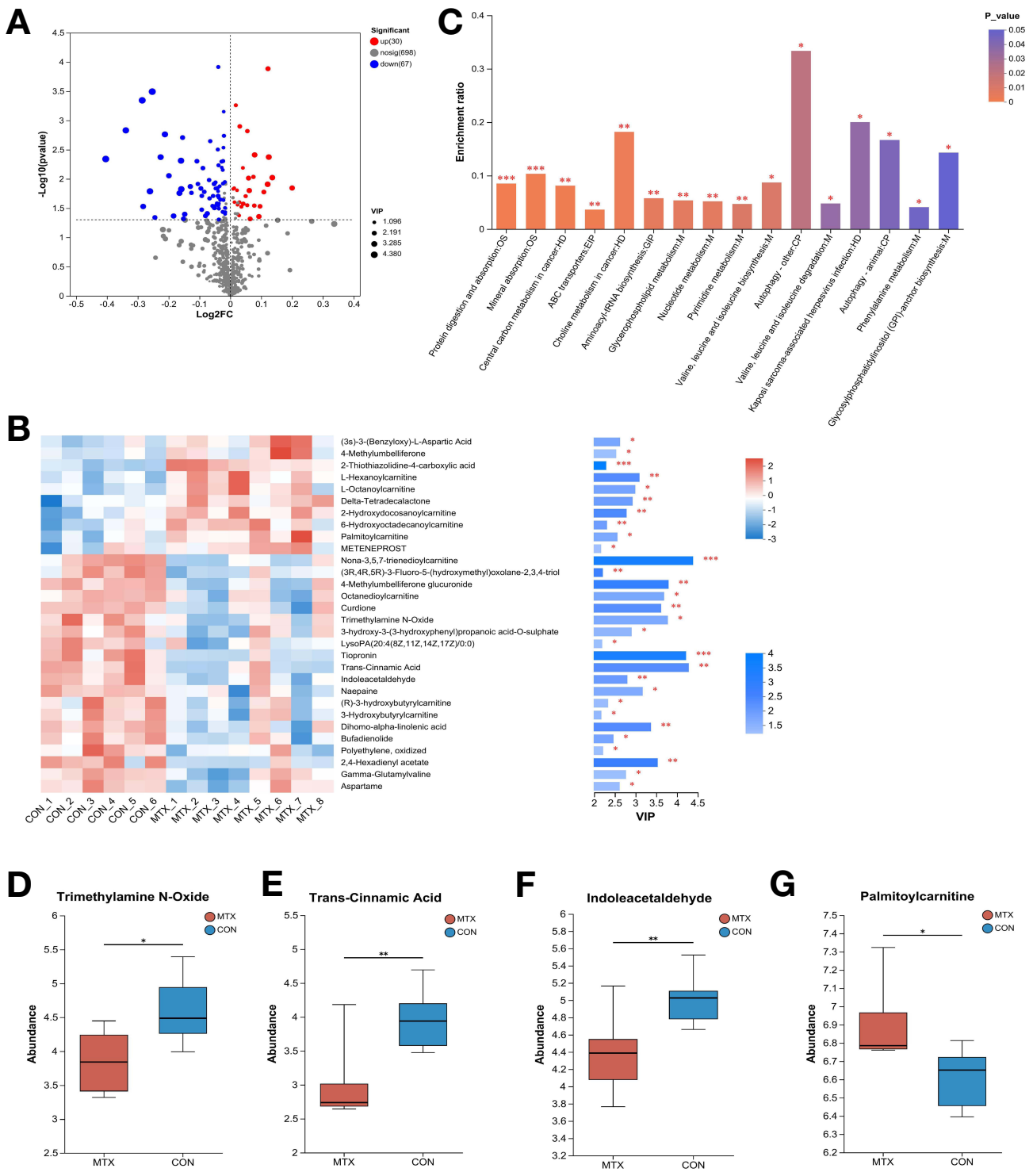

Figure 3 MTX-induced cardiac metabolomic profiles in mice. (**A**) The volcano map of differentially expressed metabolites ($p < 0.05$, and VIP > 1.0). (**B**) Heatmap of expression profile of the top (VIP) 30 of differentially expressed metabolites and their corresponding VIP values. (**C**) Overview of metabolic pathways affected by MTX ($p < 0.05$). (**D-G**) Box plots of metabolites distribution in each group of samples. *$p < 0.05$, **$p < 0.01$ and ***$p < 0.001$ represent statistically significant differences between the control and MTX groups.

norank_f__Ruminococcaceae, norank_f__Oscillospiraceae, NK4A214_group, Colidextribacter, Enterococcus, Turicibacter, and *Anaerotruncus*, were strongly correlated with distinct metabolites (cor > 0.5 or cor < −0.5). *Bacteroidota* was positively correlated with metabolites like Nona-3,5,7-trienedioylcarnitine, Trans-Cinnamic Acid (t-CA), Tiopronin, 4-Methylumbelliferone glucuronide, Octanedioylcarnitine, Curdione, and 2.4-Hexadienyl acetate

 https://doi.org/10.2147/DDDT.S479682

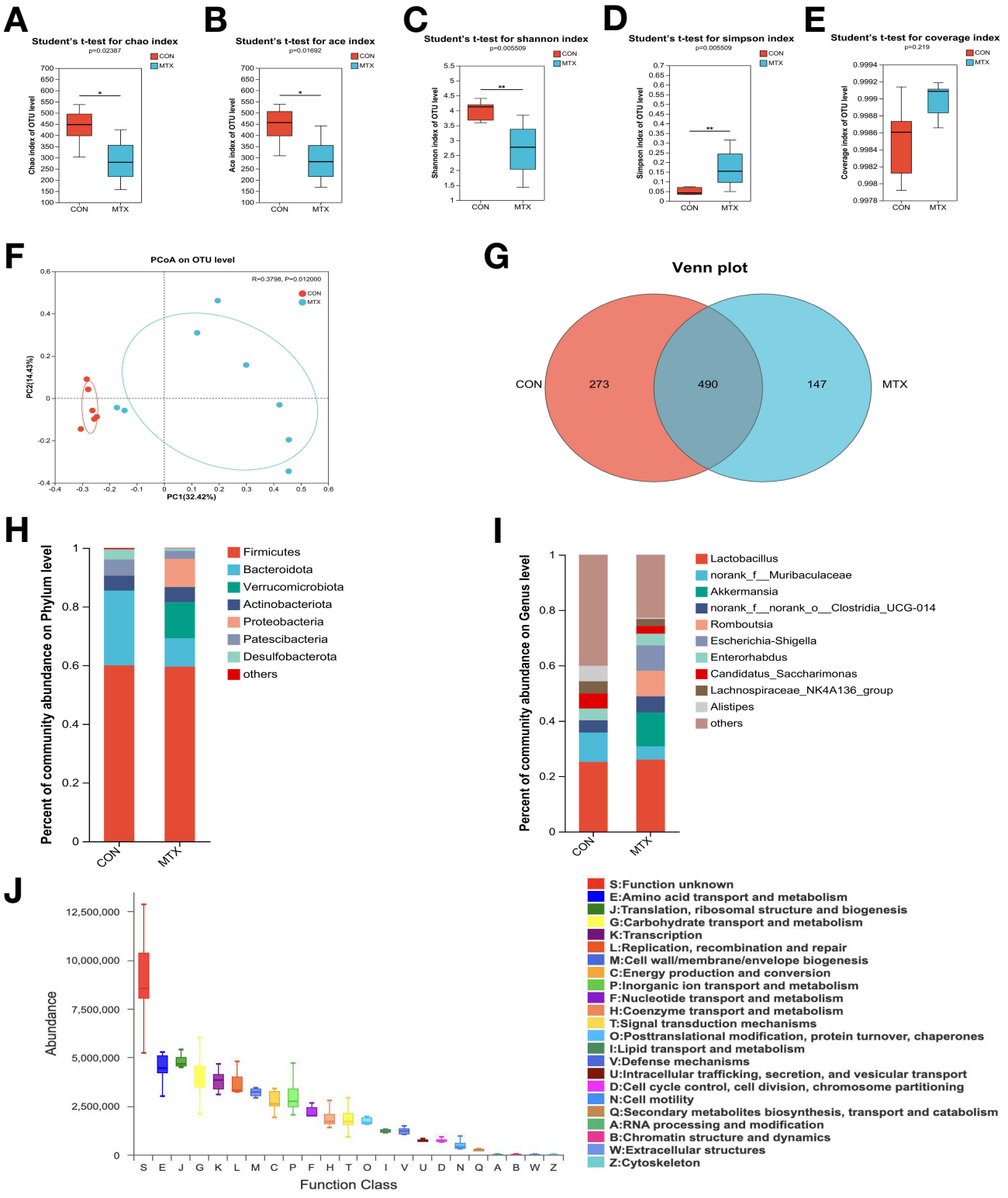

Figure 4 MTX-induced gut microbiota patterns. (**A-E**) Alpha-diversity was investigated using the Chao, Ace, Shannon, Simpson, and coverage indexes. (**F**) PCoA score plot on OTU level. (**G**) The Venn diagram analysis of OTUs. Community abundance percentages at the phylum (**H**) or genus (**I**) levels. (**J**) PICRUSt2 combined with the COG database to predict the function of gut microbiota. *$p < 0.05$ and **$p < 0.01$, compared with control group.

but negatively correlated with Palmitoylcarnitine (Figure 6). In addition, *Alistipes, norank_f__Lachnospiraceae, norank_f__Ruminococcaceae, norank_f__Oscillospiraceae, NK4A214_group, Colidextribacter*, and *Anaerotruncus* were all positively correlated with Nona-3,5,7-trienedioylcarnitine, 4-Methylumbelliferone glucuronide, and Dihomo-

https://doi.org/10.2147/DDDT.S479682

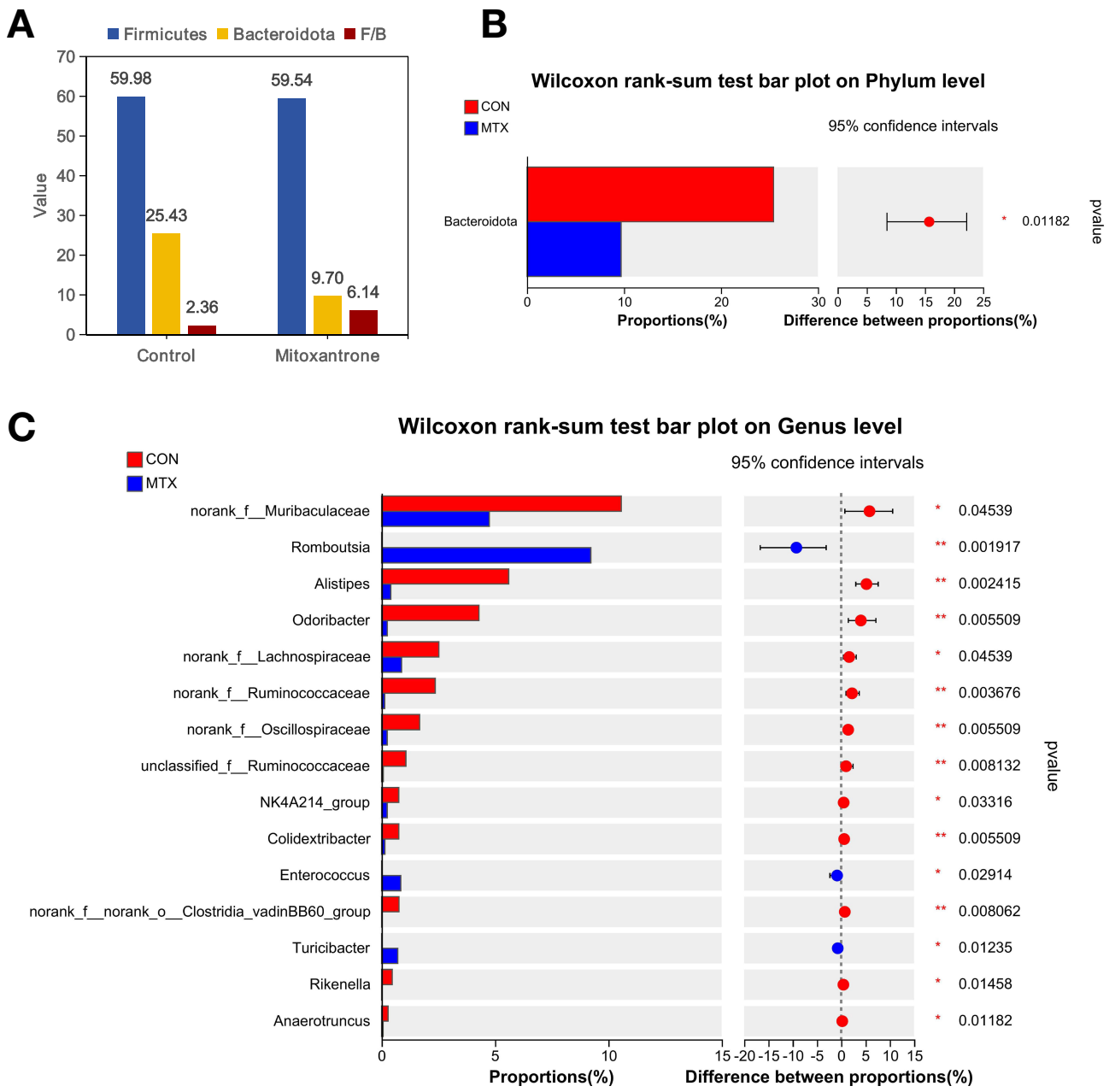

Figure 5 The significant change of MTX-induced gut microbiota components in mice. (**A**) F/B ratio of control and MTX mice samples. Wilcoxon rank-sum test bar plot for differences in species populations at the (**B**) phylum and (**C**) genus levels. *$p < 0.05$ and **$p < 0.01$ represent statistically significant differences between the control and MTX groups.

alpha-linolenic acid; while *norank_f__Lachnospiraceae, norank_f__Oscillospiraceae*, and *Colidextribacter* possessed a positive correlation with t-CA and Tiopronin. Furthermore, *Alistipes, norank_f__Ruminococcaceae*, and *NK4A214_group* possessed a positive correlation with Octanedioylcarnitine but were negatively correlated with L-Hexanoylcarnitine and L-Octanoylcarnitine. The results revealed a positive correlation between *Alistipes, Odoribacter*, and *norank_f__Ruminococcaceae* with 2.4-Hexadienyl acetate, as well as between *norank_f__Muribaculaceae, NK4A214_group*, and *Colidextribacter* with Curdione. Furthermore, *norank_f__Muribaculaceae* had a positive correlation with t-CA but was negatively correlated with Palmitoylcarnitine, whereas *Alistipes* exhibited a positive correlation with Tiopronin and TMAO but negatively correlated with (3s)-3-(Benzyloxy)-L-Aspartic Acid. The findings demonstrated a positive correlation between *Odoribacter* with

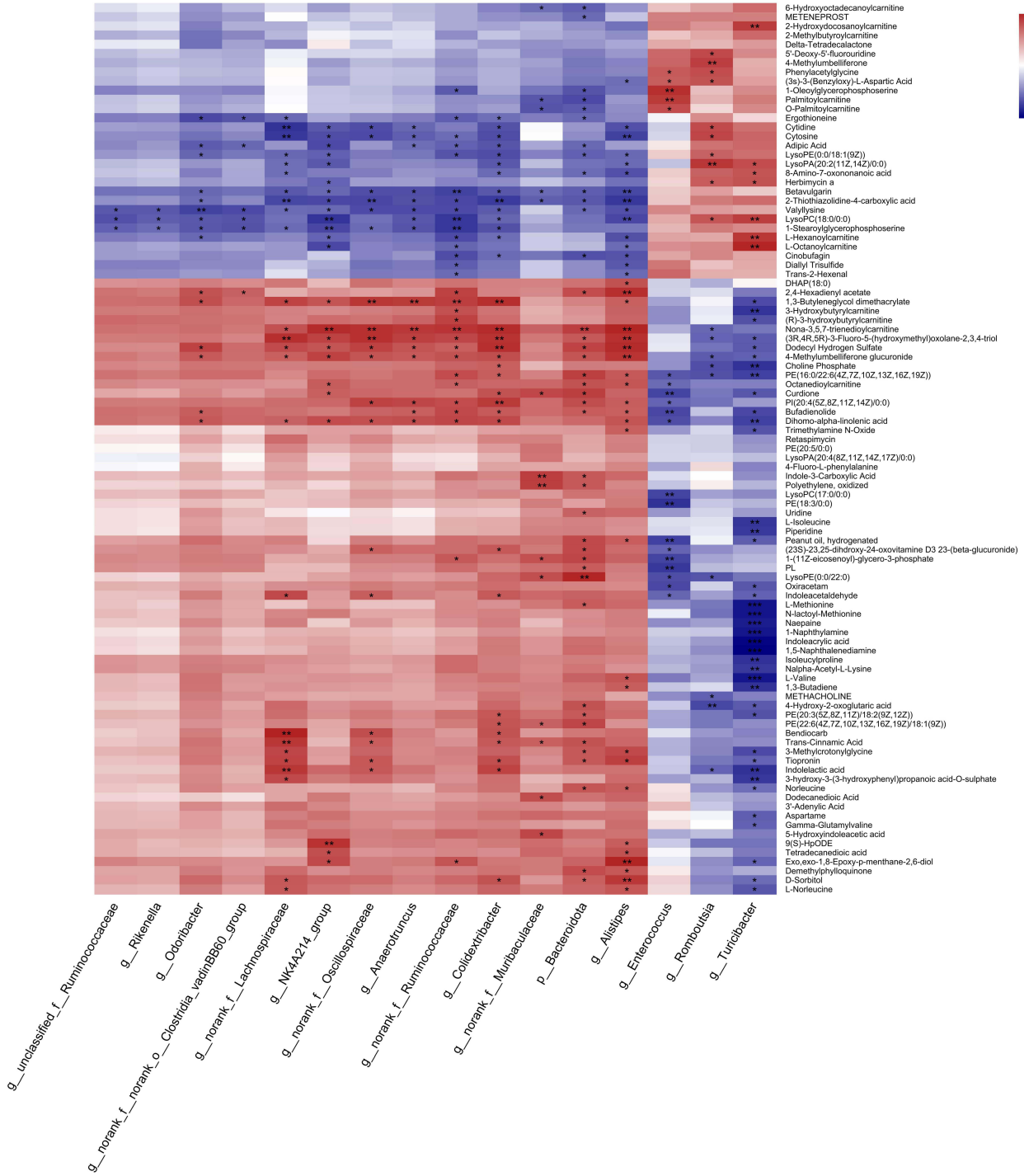

Figure 6 Pearson correlation heatmap of cardiac metabolites and gut microbiota at the phylum and genus level. Red squares represent positive correlations, blue squares represent negative correlations, and white squares represent the absence of correlations. *p < 0.05, **p < 0.01, ***p < 0.001.

4-Methylumbelliferone glucuronide and Dihomo-alpha-linolenic acid as well as between *norank_f__Lachnospiraceae* with 3-hydroxy-3-(3-hydroxyphenyl)PA-O-sulphate while indicating a negative correlation between *Colidextribacter* and L-Hexanoylcarnitine.

Our results also show that *Romboutsia* had a negative correlation with Nona-3,5,7-trienedioylcarnitine and 4-Methylumbelliferone glucuronide but a positive correlation with (3s)-3-(Benzyloxy)-L-Aspartic Acid. In addition, *Enterococcus* was negatively correlated with Octanedioylcarnitine, Curdione, Dihomo-alpha-linolenic acid, and

https://doi.org/10.2147/DDDT.S479682

Indoleacetaldehyde but positively correlated with Palmitoylcarnitine and (3s)-3-(Benzyloxy)-L-Aspartic Acid. Moreover, *Turicibacter* showed a negative correlation with Tiopronin, 4-Methylumbelliferone glucuronide, TMAO, Curdione, Dihomo-alpha-linolenic acid, Naepaine, Indoleacetaldehyde, Gamma-Glutamylvaline, 3-hydroxy-3-(3-hydroxyphenyl) PA-O-sulphate, and Aspartame but a positive correlation with L-Hexanoylcarnitine, L-Octanoylcarnitine, and 2-Hydroxydocosanoylcarnitine.

MTX-Induced Liver Immune Microenvironment Changes

After analyzing the relevance between CM biomarkers and GM, we detected the liver lymphocyte subsets to evaluate the immune state of mice after being treated with MTX. The data showed decreased $CD19^+$B cells as well as increased $CD8^+$T cells, but the increase in $CD8^+$T cells was not statistically significant. And the other subsets also had no difference between control and MTX-treated mice (Supplementary Figure 4).

Discussion

The elevated F/B ratio indicates a GM imbalance and is related to various disorders, including CVD, obesity, and diabetes.[23] Herein, MTX significantly diminished *Bacteroidetes* abundance while not significantly impacting *Firmicutes*, thereby elevating the F/B ratio. SCFAs, which have carbon chains spanning from one to six atoms, mostly result from dietary fiber fermentation in the colon.[24] SCFAs have been reported to exert a substantial impact on diverse inflammatory disorders such as hypertension and coronary artery disease, underscoring their crucial role in preserving the cardiovascular system's health.[13] At the genus level, MTX significantly decreased SCFA-producing bacteria amounts, including *norank_f__Muribaculaceae, Alistipes, Odoribacter, Colidextribacter, norank_f__norank_o__Clostridia_vadinBB60_group, Rikenella*, and *Anaerotruncus*, reducing the anti-inflammatory capacity of the system.[25–32] Additionally, MTX significantly enhanced *Enterococcus, Romboutsia*, and *Turicibacter* abundances. *Enterococcus*, an important opportunistic pathogen, naturally colonizes the gastrointestinal tract in most humans and animals.[33] *Enterococcus* has been demonstrated to interrupt the intestinal barrier and induce macrophage activation through the nuclear factor kappa B (NF-κB) pathway activation besides secreting inflammatory cytokines.[34] Meanwhile, elevated intestinal permeability has enhanced microorganism translocation, metabolites, and inflammatory factors into system circulation through the portal vein, thus instigating systemic inflammatory response.[35] Moreover, MTX significantly lowered *norank_f__Muribaculaceae, Alistipes, norank_f__Lachnospiraceae*, and *norank_f__Ruminococcaceae* genera amounts, which are negatively related to pro-inflammatory cytokine secretion levels. This further implies that MTX provoked inflammation that was a characteristic risk factor for CVD and consequently increased the incident MTX-induced cardiotoxicity risks.[25,36–40] Consistently, MTX administration has been documented to significantly alter pro-inflammatory cytokine expression, increasing tumor necrosis factor-alpha and decreasing interleukin-6 in mouse cardiac tissue, suggesting the probable role of inflammation in triggering MTX-provoked cardiotoxicity.[16] In addition, several CVDs share some frequent pathophysiologic pathways, including endothelial malfunction.[41] Yin et al identified a correlation between the decreased abundance of *Romboutsia* and enhancements in vascular endothelial function, suggesting that *Romboutsia* may induce endothelial dysfunction, thereby contributing to the emergence and progression of cardiotoxicity associated with MTX.[42]

TMAO represents another pivotal gut microbial metabolite, with dietary intake playing a crucial role in its formation. Choline, L-carnitine, betaine, and other compounds that contain choline are first metabolized by gut microbes that have trimethylamine (TMA) lyase, resulting in TMA production. This TMA is then transformed into TMAO through hepatic flavin monooxygenase 3 (FMO3).[43] Consequently, dietary intake, gut microbial composition, and hepatic FMO3 expression all influence the TMAO levels in the body. Studies have demonstrated a close relation between elevated circulating levels of TMAO and CVD risk stratification and mortality.[44] Evidence has shown a significant plasma TMAO levels have an inverse relationship with the relative *Anaerotruncus* abundance and a notable positive correlation with the relative abundance of *Turicibacter*.[45,46] Herein, the MTX group mice exhibited TMAO downregulation and liver injury. Moreover, at the genus level, circulating TMAO levels did not have a correlation with the relative *Anaerotruncus* abundance while having a significant reverse association with the relative *Turicibacter* abundance. Therefore, we speculate that MTX may reduce hepatic FMO3 expression, leading to impaired TMA oxidation, decreased TMAO

formation, and consequently altering the correlation between TMAO, Anaerotruncus, and Turicibacter. This also suggests that the mechanism of cardiotoxicity induced by MTX might differ from the cardiac injury mechanisms in CVDs.[47]

The t-CA, a gut microbial metabolite of phenylalanine, has various anti-inflammatory, anticancer, and antioxidant biological activities.[48,49] t-CA enhances nuclear factor E2-correlated factor 2 nuclear translocation that is accompanied by upregulated antioxidant genes.[50] In addition, t-CA has been found to be an inhibitor of HDACs.[49] HADCs have a crucial role in controlling the activity of genes that are commonly activated throughout inflammation, indicating that HDACs have a direct impact on the inflammatory process.[51] Notably, HDAC expression has a close relation to multiple heart disease characteristics, including myocardial fibrosis and hypertrophy, cardiac dysfunction, arrhythmia, ventricular dilatation, and post-myocardial infarction apoptosis.[52] This study represented that t-CA downregulated significantly in the MTX group mice, and the decreased *norank_f__Lachnospiraceae, norank_f__Oscillospiraceae, Colidextribacter*, and *norank_f__Muribaculaceae* genera abundances after the MTX challenge exhibited a positive correlation with t-CA presence. This implies that MTX-triggered GM changes in our mice may have impacted phenylalanine metabolism, which attenuated the body's anti-inflammatory and antioxidant capacities and caused abnormal activity of HDACs, hence mediating cardiotoxicity.

Indole and its derivatives, essential GM-derived tryptophan (Trp) metabolites, are specific aryl hydrocarbon receptor (AhR) ligands that have the capability of activating the AhR pathway.[53] AhR activation is involved in maintaining intestinal homeostasis and governing intestinal immunity and inflammation.[54] Furthermore, Trp metabolites and the AhR help prevent detrimental cardiac remodeling and systolic malfunction in heart failure.[55] Here, the MTX group mice exhibited a significant downregulation of GM-derived Trp metabolites that included indole-3-carboxylic acid, indole acetaldehyde, indole acrylic acid, and indole lactic acid. Moreover, Trp metabolite presence was positively correlated with the decreased *norank_f__Lachnospiraceae, norank_f__Oscillospiraceae, Colidextribacter*, and *norank_f__Muribaculaceae* genera abundances and negatively correlated with increased *Romboutsia, Enterococcus*, and *Turicibacter* abundances post-MTX challenge. This indicates that MTX-triggered GM alternations in our mice may have impacted Trp metabolism, mediating enterotoxicity and cardiotoxicity.

Dihomo-alpha-linolenic acid, or 11,14,17-eicosatrienoic acid, constitutes a scarce omega-3 polyunsaturated fatty acid (FA). Eicosatrienoic acid shows anti-inflammatory properties through NF-κB activity downregulation.[56] In addition, Gamma-Glutamylvaline has been identified as an anti-inflammatory peptide due to its earlier demonstrated ability to reduce inflammation in vascular, gastrointestinal, and adipocyte tissues.[57–59] In our study, we found Dihomo-alpha-linolenic acid and Gamma-Glutamylvaline downregulated in the MTX group mice. The increased *Turicibacter* genus abundance was negatively correlated with Gamma-Glutamylvaline presence. Meanwhile, Dihomo-alpha-linolenic acid presence was negatively correlated with the increased *Enterococcus* and *Turicibacter* genera abundances and positively correlated with the decreased *Alistipes, Odoribacter, Colidextribacter, norank_f__Lachnospiraceae, NK4A214_group, norank_f__Ruminococcaceae, norank_f__Oscillospiraceae*, and *Anaerotruncus* genera abundances. This indicates again that MTX-triggered GM modifications in our mice may have weakened the body's anti-inflammatory capacity.

Cardiomyocytes prioritize the utilization of FA oxidation for energy supply, and ACs are intermediate metabolites of FA β-oxidation. ACs are elevated considerably in the serum and plasma due to mitochondrial dysfunction.[60] Peroxisomes constitute the primary organelles responsible for the metabolism of VLC-FAs and the synthesis of shorter ACs. Hence, the elevated concentrations of circulating VLC-ACs could potentially be associated with peroxisomal dysfunction.[61] In our study, accumulation of various long-chain and VLC-ACs was observed post-MTX challenge, and we found the genus *norank_f__Muribaculaceae* to be negative with various long-chain ACs such as palmitoylcarnitine, O-palmitoylcarnitine, and 6-hydroxyoctadecanoylcarnitine, *Enterococcus* to be positively correlated with palmitoylcarnitine and O-palmitoylcarnitine, and *Turicibacter* to be positively correlated with 2-hydroxydocosanoylcarnitine, a VLC-AC, suggesting that MTX-triggered GM alternations in our mice may have impacted mitochondrial and peroxisomes function and cardiac energetic metabolism. Meanwhile, the accumulation of these ACs further exacerbates cardiac dysfunction and promotes the development of MTX-induced cardiotoxicity.[62,63] In addition, we also found partial medium-chain ACs such as nona-3,5,7-trienedioylcarnitine and octanedioylcarnitine downregulated significantly in the MTX group mice, but the specific function is still unclear until now.

Autophagy is a crucial heart cellular process that eliminates protein aggregates and damaged organelles. It provides protection against conditions such as excessive β-adrenergic stimulation, famine, and ischemia.[64] Herein, various phosphatidylethanolamines (PEs) exhibiting enrichment in the autophagy pathway, including PE(16:0/22:6(4Z,7Z,10Z,13Z,16Z,19Z)), PE(22:6(4Z,7Z,10Z,13Z,16Z,19Z)/18:1(9Z)) and PE(20:3(5Z,8Z,11Z)/18:2(9Z,12Z)) were downregulated in the MTX group mice, suggesting that MTX blocked this autophagy route. This aligns with an existing study showing that MTX suppressed autophagy by reducing the levels of key autophagy proteins in adult male CD-1 mice, specifically microtubule-related protein light chain 3 B (LC3B), Beclin1, and autophagy protein 5.[65] Nevertheless, Reis-Mendes et al demonstrated that autophagy was involved in MTX-provoked cytotoxicity in differentiated AC16 cardiac cells, with MTX seeming to be an autophagy inducer, probably via sequestosome-1 (p62)/LC3B-II incorporation.[66] In addition, we found that autophagy had a positive correlation with *Colidextribacter, norank_f__Ruminococcaceae, norank_f__Muribaculaceae*, and *Alistipes* genera, and a negative correlation with *Romboutsia, Enterococcus*, and *Turicibacter* in the heart. Our results, for the first time, clarify that MTX can downregulate autophagy in the heart based on metabolomics, and it must be looked at further elucidating autophagy's role in MTX-provoked cardiotoxicity.

Currently, gastrointestinal toxicity is one of the primary causes of unsuccessful outcomes of chemotherapy. This detrimental consequence results in a decrease in dosage and cessation of the therapy cycle, which has a negative impact on the therapeutic outcomes of chemotherapy.[67] Here, several amino acids enriched in the protein digestion and absorption along with the mineral absorption pathways, such as L-Isoleucine, L-Methionine, and L-Valine, exhibited a downregulation in the MTX group mice, revealing the disruption of digestive system functions post-MTX challenge. Moreover, these two pathways negatively correlated with the *Turicibacter* genus and positively correlated with *Alistipes*. Additionally, we elucidated changed metabolic pathways besides these two previously mentioned pathways, including central carbon and choline metabolism in neoplasm, ABC transporters, aminoacyl-tRNA biosynthesis, and glycerophospholipid, nucleotide, and pyrimidine metabolism. The results corresponded to our COG function prediction, demonstrating that MTX impacted amino acid transport and metabolism, carbohydrates, inorganic ions, nucleotides, and coenzymes. It also affected processes such as translation, transcription, replication, ribosomal structure, recombination, biogenesis, and repair. Additionally, MTX influenced the biogenesis of cell walls, membranes, and envelopes, as well as energy production and conversion.

Our main aim was to conduct an initial evaluation of the possible mechanisms by which MTX may trigger cardiotoxicity. We discovered correlations between changes in GM and alterations in cardiac metabolites. However, it is still crucial to identify the key bacteria and metabolites involved in this process. Researchers should perform fecal bacteria transplantation investigations to confirm the validity of our findings.

Conclusions

MTX exposure results in cardiotoxicity related to GM and metabolomic pathway alternations. MTX increased *Romboutsia, Enterococcus*, and *Turicibacter* abundances and decreased *norank_f__Muribaculaceae, Alistipes, Odoribacter, norank_f__Lachnospiraceae, norank_f__Ruminococcaceae, norank_f__Oscillospiraceae, unclassified_f__Ruminococcaceae, NK4A214_group, Colidextribacter, norank_f__norank_o__Clostridia_vadinBB60_group, Rikenella*, and *Anaerotruncus* abundances. Additionally, MTX primarily disturbed the processes of mineral absorption, protein digestion and absorption, membrane transport, aminoacyl-tRNA production, amino acid, lipid, and nucleotide metabolism, as well as autophagy. Correlation analyses offer a viable method to comprehensively comprehend the cardiotoxic effects caused by MTX.

Institutional Review Board Statement

The animal study protocol was approved by the Ethics Committee of Jining NO.1 People's Hospital on 23 August 2023 (2023DW090). This research project was approved by the Ethics Committee of Jining NO.1 People's Hospital and was conducted in strict accordance with ethical guidelines.

Funding

This research was funded by Key R&D Program of Jining (2023YXNS019).

Disclosure

The authors declare no conflicts of interest in this work.

References

1. Bu YZ, Xu JR, Luo Q, et al. A precise nanostructure of folate-overhung mitoxantrone DNA tetrahedron for targeted capture leukemia. *Nanomaterials (Basel)*. 2020;10(5):951. doi:10.3390/nano10050951
2. Seiter K. Toxicity of the topoisomerase II inhibitors. *Expert Opin Drug Saf*. 2005;4(2):219–234. doi:10.1517/14740338.4.2.219
3. Lucarini V, Melaiu O, D'Amico S, et al. Combined mitoxantrone and anti-TGFβ treatment with PD-1 blockade enhances antitumor immunity by remodelling the tumor immune landscape in neuroblastoma. *J Exp Clin Cancer Res*. 2022;41(1):326. doi:10.1186/s13046-022-02525-9
4. Fox EJ. Mechanism of action of mitoxantrone. *Neurology*. 2004;63(12 Suppl 6):S15–8. doi:10.1212/wnl.63.12_suppl_6.s15
5. Reis-Mendes AF, Sousa E, de Lourdes Bastos M, Costa VM. The role of the metabolism of anticancer drugs in their induced-cardiotoxicity. *Curr Drug Metab*. 2015;17(1):75–90. doi:10.2174/1389200216666151103114926
6. Shaikh AY, Suryadevara S, Tripathi A, et al. Mitoxantrone-induced cardiotoxicity in acute myeloid leukemia-a velocity vector imaging analysis. *Echocardiography*. 2016;33(8):1166–1177. doi:10.1111/echo.13245
7. Thomas X, Le QH, Fiere D. Anthracycline-related toxicity requiring cardiac transplantation in long-term disease-free survivors with acute promyelocytic leukemia. *Ann Hematol*. 2002;81(9):504–507. doi:10.1007/s00277-002-0534-8
8. Gilbert JA, Blaser MJ, Caporaso JG, et al. Current understanding of the human microbiome. *Nat Med*. 2018;24(4):392–400. doi:10.1038/nm.4517
9. Qin J, Li R, Raes J, et al. A human gut microbial gene catalogue established by metagenomic sequencing. *Nature*. 2010;464(7285):59–65. doi:10.1038/nature08821
10. Feng Q, Liu Z, Zhong S, et al. Integrated metabolomics and metagenomics analysis of plasma and urine identified microbial metabolites associated with coronary heart disease. *Sci Rep*. 2016;6(1):22525. doi:10.1038/srep22525
11. Razavi AC, Potts KS, Kelly TN, Bazzano LA. Sex, gut microbiome, and cardiovascular disease risk. *Biol Sex Differ*. 2019;10(1):29. doi:10.1186/s13293-019-0240-z
12. Nogal A, Valdes M, Menni C. The role of short-chain fatty acids in the interplay between gut microbiota and diet in cardio-metabolic health. *Gut Microbes*. 2021;13(1):1–24. doi:10.1080/19490976.2021.1897212
13. Zhang Z, Zhang H, Chen T, et al. Regulatory role of short-chain fatty acids in inflammatory bowel disease. *Cell Commun Signal*. 2022;20(1):64. doi:10.1186/s12964-022-00869-5
14. Andersson BS, Eksborg S, Vidal RF, et al. Anthraquinone-induced cell injury: acute toxicity of carminomycin, epirubicin, idarubicin and mitoxantrone in isolated cardiomyocytes. *Toxicology*. 1999;135(1):11–20. doi:10.1016/s0300-483x(99)00041-4
15. Rossato LG, Costa VM, de Pinho PG, et al. The metabolic profile of mitoxantrone and its relation with mitoxantrone-induced cardiotoxicity. *Arch Toxicol*. 2013;87(10):1809–1820. doi:10.1007/s00204-013-1040-6
16. Reis-Mendes A, Dores-Sousa JL, Padrão AI, et al. Inflammation as a possible trigger for mitoxantrone-induced cardiotoxicity: an in vivo study in adult and infant mice. *Pharmaceuticals (Basel)*. 2021;14(6):510. doi:10.3390/ph14060510
17. Rossato LG, Costa VM, Dallegrave E, et al. Mitochondrial cumulative damage induced by mitoxantrone: late onset cardiac energetic impairment. *Cardiovasc Toxicol*. 2014;14(1):30–40. doi:10.1007/s12012-013-9230-2
18. Costa VM, Capela JP, Sousa JR, et al. Mitoxantrone impairs proteasome activity and prompts early energetic and proteomic changes in HL-1 cardiomyocytes at clinically relevant concentrations. *Arch Toxicol*. 2020;94(12):4067–4084. doi:10.1007/s00204-020-02874-4
19. Belli M, Barone L, Longo S, et al. Gut microbiota composition and cardiovascular disease: a potential new therapeutic target? *Int J mol Sci*. 2023;24(15):11971. doi:10.3390/ijms241511971
20. Desai MS, Seekatz AM, Koropatkin NM, et al. A dietary fiber-deprived gut microbiota degrades the colonic mucus barrier and enhances pathogen susceptibility. *Cell*. 2016;167(5):1339–1353.e21. doi:10.1016/j.cell.2016.10.043
21. Marques FZ, Nelson E, Chu PY, et al. High-fiber diet and acetate supplementation change the gut microbiota and prevent the development of hypertension and heart failure in hypertensive mice. *Circulation*. 2017;135(10):964–977. doi:10.1161/circulationaha.116.024545
22. Gan XT, Ettinger G, Huang CX, et al. Probiotic administration attenuates myocardial hypertrophy and heart failure after myocardial infarction in the rat. *Circ Heart Fail*. 2014;7(3):491–499. doi:10.1161/circheartfailure.113.000978
23. Everard A, Cani PD. Diabetes, obesity and gut microbiota. *Best Pract Res Clin Gastroenterol*. 2013;27(1):73–83. doi:10.1016/j.bpg.2013.03.007
24. Hu T, Wu Q, Yao Q, et al. Short-chain fatty acid metabolism and multiple effects on cardiovascular diseases. *Ageing Res Rev*. 2022;81:101706. doi:10.1016/j.arr.2022.101706
25. Dong F, Xiao F, Li X, et al. Pediococcus pentosaceus CECT 8330 protects DSS-induced colitis and regulates the intestinal microbiota and immune responses in mice. *J Transl Med*. 2022;20(1):33. doi:10.1186/s12967-022-03235-8
26. He J, Guo K, Chen Q, Wang Y. Camel milk modulates the gut microbiota and has anti-inflammatory effects in a mouse model of colitis. *J Dairy Sci*. 2022;105(5):3782–3793. doi:10.3168/jds.2021-21345
27. Liu X, Tong X, Zou Y, et al. Mendelian randomization analyses support causal relationships between blood metabolites and the gut microbiome. *Nat Genet*. 2022;54(1):52–61. doi:10.1038/s41588-021-00968-y
28. Louis P, Duncan SH, McCrae SI, et al. Restricted distribution of the butyrate kinase pathway among butyrate-producing bacteria from the human colon. *J Bacteriol*. 2004;186(7):2099–2106. doi:10.1128/jb.186.7.2099-2106.2004
29. Wang Q, Wang C, Abdullah Tian W, et al. Hydroxytyrosol alleviates dextran sulfate sodium-induced colitis by modulating inflammatory responses, intestinal barrier, and microbiome. *J Agric Food Chem*. 2022;70(7):2241–2252. doi:10.1021/acs.jafc.1c07568
30. Xu S, Jiao C, Diao Q, Tu Y. Preweaning period is a critical window for rumen microbial regulation of average daily gain in Holstein heifer calves. *J Anim Sci Biotechnol*. 2023;14(1):128. doi:10.1186/s40104-023-00934-0
31. Shi H, Chang Y, Gao Y, et al. Dietary fucoidan of Acaudina molpadioides alters gut microbiota and mitigates intestinal mucosal injury induced by cyclophosphamide. *Food Funct*. 2017;8(9):3383–3393. doi:10.1039/c7fo00932a

32. Zhao S, Peng X, Zhou QY, et al. Bacillus coagulans 13002 and fructo-oligosaccharides improve the immunity of mice with immunosuppression induced by cyclophosphamide through modulating intestinal-derived and fecal microbiota. *Food Res Int*. 2021;140:109793. doi:10.1016/j.foodres.2020.109793
33. Arias CA, Murray BE. The rise of the Enterococcus: beyond vancomycin resistance. *Nat Rev Microbiol*. 2012;10(4):266–278. doi:10.1038/nrmicro2761
34. Zhang X, Liang Y, Jiang J, et al. A high-salt diet exacerbates liver fibrosis through enterococcus-dependent macrophage activation. *Microbiol Spectr*. 2023;11(2):e0340322. doi:10.1128/spectrum.03403-22
35. Camilleri M. Leaky gut: mechanisms, measurement and clinical implications in humans. *Gut*. 2019;68(8):1516–1526. doi:10.1136/gutjnl-2019-318427
36. Wang H, Huang J, Ding Y, et al. Nanoparticles isolated from porcine bone soup ameliorated dextran sulfate sodium-induced colitis and regulated gut microbiota in mice. *Front Nutr*. 2022;9:821404. doi:10.3389/fnut.2022.821404
37. Wu M, Li P, An Y, et al. Phloretin ameliorates dextran sulfate sodium-induced ulcerative colitis in mice by regulating the gut microbiota. *Pharmacol Res*. 2019;150:104489. doi:10.1016/j.phrs.2019.104489
38. Wang K, Li W, Wang K, et al. Litchi thaumatin-like protein induced the liver inflammation and altered the gut microbiota community structure in mice. *Food Res Int*. 2022;161:111868. doi:10.1016/j.foodres.2022.111868
39. Zhao N, Wang Y, Ma Y, et al. Jia-Wei-Si-Miao-Yong-An decoction modulates intestinal flora and metabolites in acute coronary syndrome model. *Front Cardiovasc Med*. 2022;9:1038273. doi:10.3389/fcvm.2022.1038273
40. Bui TVA, Hwangbo H, Lai Y, et al. The gut-heart axis: updated review for the roles of microbiome in cardiovascular health. *Korean Circ J*. 2023;53(8):499–518. doi:10.4070/kcj.2023.0048
41. Zuo K, Li J, Li K, et al. Disordered gut microbiota and alterations in metabolic patterns are associated with atrial fibrillation. *Gigascience*. 2019;8(6). doi:10.1093/gigascience/giz058
42. Yin H, Huang J, Guo X, et al. Romboutsia lituseburensis JCM1404 supplementation ameliorated endothelial function via gut microbiota modulation and lipid metabolisms alterations in obese rats. *FEMS Microbiol Lett*. 2023;370. doi:10.1093/femsle/fnad016.
43. Ma J, Li H. The role of gut microbiota in atherosclerosis and hypertension. *Front Pharmacol*. 2018;9:1082. doi:10.3389/fphar.2018.01082
44. Qi J, You T, Li J, et al. Circulating trimethylamine N-oxide and the risk of cardiovascular diseases: a systematic review and meta-analysis of 11 prospective cohort studies. *J Cell Mol Med*. 2018;22(1):185–194. doi:10.1111/jcmm.13307
45. Shirouchi B, Fukuda A, Akasaka T. Unlike glycerophosphocholine or choline chloride, dietary phosphatidylcholine does not increase plasma trimethylamine-n-oxide levels in Sprague-Dawley rats. *Metabolites*. 2022;12(1):64. doi:10.3390/metabo12010064
46. O'Connor A, Quizon PM, Albright JE, et al. Responsiveness of cardiometabolic-related microbiota to diet is influenced by host genetics. *Mamm Genome*. 2014;25(11–12):583–599. doi:10.1007/s00335-014-9540-0
47. Thonusin C, Nawara W, Khuanjing T, et al. Blood metabolomes as non-invasive biomarkers and targets of metabolic interventions for doxorubicin and trastuzumab-induced cardiotoxicity. *Arch Toxicol*. 2023;97(2):603–618. doi:10.1007/s00204-022-03412-0
48. Oliphant K, Allen-Vercoe E. Macronutrient metabolism by the human gut microbiome: major fermentation by-products and their impact on host health. *Microbiome*. 2019;7(1):91. doi:10.1186/s40168-019-0704-8
49. Zhu B, Shang B, Li Y, Zhen Y. Inhibition of histone deacetylases by trans-cinnamic acid and its antitumor effect against colon cancer xenografts in athymic mice. *Mol Med Rep*. 2016;13(5):4159–4166. doi:10.3892/mmr.2016.5041
50. Hseu YC, Korivi M, Lin FY, et al. Trans-cinnamic acid attenuates UVA-induced photoaging through inhibition of AP-1 activation and induction of Nrf2-mediated antioxidant genes in human skin fibroblasts. *J Dermatol Sci*. 2018;90(2):123–134. doi:10.1016/j.jdermsci.2018.01.004
51. Kulthinee S, Yano N, Zhuang S, et al. Critical Functions of Histone Deacetylases (HDACs) in modulating inflammation associated with cardiovascular diseases. *Pathophysiology*. 2022;29(3):471–485. doi:10.3390/pathophysiology29030038
52. Jin G, Wang K, Zhao Y, et al. Targeting histone deacetylases for heart diseases. *Bioorg Chem*. 2023;138:106601. doi:10.1016/j.bioorg.2023.106601
53. Lamas B, Natividad JM, Sokol H. Aryl hydrocarbon receptor and intestinal immunity. *Mucosal Immunol*. 2018;11(4):1024–1038. doi:10.1038/s41385-018-0019-2
54. Zhou R, He D, Xie J, et al. The synergistic effects of polysaccharides and ginsenosides from American Ginseng (panax quinquefolius l.) ameliorating cyclophosphamide-induced intestinal immune disorders and gut barrier dysfunctions based on microbiome-metabolomics analysis. *Front Immunol*. 2021;12:665901. doi:10.3389/fimmu.2021.665901
55. Carrillo-Salinas FJ, Anastasiou M, Ngwenyama N, et al. Gut dysbiosis induced by cardiac pressure overload enhances adverse cardiac remodeling in a T cell-dependent manner. *Gut Microbes*. 2020;12(1):1–20. doi:10.1080/19490976.2020.1823801
56. Huang WC, Tsai PJ, Huang YL, et al. PGE2 production is suppressed by chemically-synthesized Δ7-eicosatrienoic acid in macrophages through the competitive inhibition of COX-2. *Food Chem Toxicol*. 2014;66:122–133. doi:10.1016/j.fct.2014.01.031
57. Guha S, Paul C, Alvarez S, et al. Dietary γ-glutamyl valine ameliorates tnf-α-induced vascular inflammation via endothelial calcium-sensing receptors. *J Agric Food Chem*. 2020;68(34):9139–9149. doi:10.1021/acs.jafc.0c04526
58. Zhang H, Kovacs-Nolan J, Kodera T, et al. γ-Glutamyl cysteine and γ-glutamyl valine inhibit TNF-α signaling in intestinal epithelial cells and reduce inflammation in a mouse model of colitis via allosteric activation of the calcium-sensing receptor. *Biochim Biophys Acta*. 2015;1852(5):792–804. doi:10.1016/j.bbadis.2014.12.023
59. Xing L, Zhang H, Majumder K, et al. γ-glutamylvaline prevents low-grade chronic inflammation via activation of a calcium-sensing receptor pathway in 3T3-L1Mouse adipocytes. *J Agric Food Chem*. 2019;67(30):8361–8369. doi:10.1021/acs.jafc.9b02334
60. Wang J, Sun Y, Teng S, Li K. Prediction of sepsis mortality using metabolite biomarkers in the blood: a meta-analysis of death-related pathways and prospective validation. *BMC Med*. 2020;18(1):83. doi:10.1186/s12916-020-01546-5
61. Duranti G, Boenzi S, Rizzo C, et al. Urine acylcarnitine analysis by ESI-MS/MS: a new tool for the diagnosis of peroxisomal biogenesis disorders. *Clin Chim Acta*. 2008;398(1–2):86–89. doi:10.1016/j.cca.2008.08.018
62. Mutomba MC, Yuan H, Konyavko M, et al. Regulation of the activity of caspases by L-carnitine and palmitoylcarnitine. *FEBS Lett*. 2000;478(1–2):19–25. doi:10.1016/s0014-5793(00)01817-2
63. Shao Y, Redfors B, Benoist D, et al. Lipid metabolites and their differential pro-arrhythmic profiles: of importance in the development of a new anti-arrhythmic pharmacology. *mol Cell Biochem*. 2014;393(1–2):191–197. doi:10.1007/s11010-014-2060-0

64. De Meyer GR, Martinet W. Autophagy in the cardiovascular system. *Biochim Biophys Acta*. 2009;1793(9):1485–1495. doi:10.1016/j.bbamcr.2008.12.011
65. Brandão SR, Reis-Mendes A, Duarte-Araújo M, et al. Cardiac molecular remodeling by anticancer drugs: doxorubicin affects more metabolism while mitoxantrone impacts more autophagy in adult CD-1 male mice. *Biomolecules*. 2023;13(6):921. doi:10.3390/biom13060921
66. Reis-Mendes A, Carvalho F, Remião F, et al. Autophagy (but not metabolism) is a key event in mitoxantrone-induced cytotoxicity in differentiated AC16 cardiac cells. *Arch Toxicol*. 2023;97(1):201–216. doi:10.1007/s00204-022-03363-6
67. Boussios S, Pentheroudakis G, Katsanos K, Pavlidis N. Systemic treatment-induced gastrointestinal toxicity: incidence, clinical presentation and management. *Ann Gastroenterol*. 2012;25(2):106–118.